Contents lists available at ScienceDirect

International Journal of Applied Earth Observation and Geoinformation

journal homepage: www.elsevier.com/locate/jag

Boreal tree species classification using airborne laser scanning data annotated with harvester production reports, and convolutional neural networks

Raul de Paula Pires *, Christoffer Axelsson, Eva Lindberg, Henrik Jan Persson, Kenneth Olofsson, Johan Holmgren

Dept. of Forest Resource Management. Swedish University of Agricultural Sciences, Umeå, Sweden

ARTICLE INFO

Keywords:
Tree species classification
Convolutional neural networks
Aerial laser scanning
Dual-wavelength
Harvester data

ABSTRACT

This study explores the potential of spatially explicit Harvester Production Reports (HPRs) for automatic annotation of Aerial Laser Scanning (ALS) data at tree-level, enabling accurate tree species classification using Convolutional Neural Networks (CNNs). By integrating HPRs into the modelling process, this approach provides a practical solution for addressing challenges in remote sensing data annotation for forestry applications. The ALS data were acquired in managed Norway spruce-dominated forests in southern Sweden using a dual-wavelength system composed by two monochromatic sensors. Thus, three datasets were produced: the 905 nm miniVUX dataset (~100 points/m^2), the 1550 nm VUX dataset (~875 points/m^2), and the dual-wavelength dataset (~975 points/m^2), the last being a junction of the two first datasets. The automatic annotation was performed by matching tree records in the HPR and ALS data based on spatial proximity and height similarity, with a total of 45,516 HPR-recorded tree positions being linked to ALS-derived segments and assigned species labels based on HPR records. Then, the individual tree-level ALS point clouds were converted into 2D images from multiple viewing angles, with varying image dimensions and pixel sizes to accommodate trees of different sizes. These images served as input for CNN-based classification, enabling species identification across ALS datasets with varying spectral and spatial resolutions. The CNN models were trained and evaluated to classify trees into Norway spruce, Scots pine, Deciduous, and a "Noise" class for segmentation errors. The classification accuracy varied according to the dataset used, with the dual-wavelength dataset achieving the highest macro-F1 score (0.896), followed by the VUX dataset (0.894) and miniVUX dataset (0.835). These findings highlight spatially explicit HPRs as efficient, high-quality reference data for CNN-based tree species classification with minimal annotation effort.

1. Introduction

Precision forestry applications integrate remote sensing technologies and estimation techniques to enhance sustainable forest management. By providing detailed insights into tree-level attributes like tree health and timber quality, they allow informed decision-making and optimal resource allocation (Fardusi et al., 2017; Fassnacht et al., 2024). Commonly, precision forestry is supported by advanced remote sensing technologies, such as Light Detection and Ranging (LiDAR) sensors, and high resolution aerial imagery, which are used to collect detailed data on forests and enable the retrieval of information at individual tree-level. (Holopainen et al., 2014).

A key component of such forest assessments is the accurate estimation of tree species composition, which plays a critical role in management and conservation efforts (Fassnacht et al., 2016; Yu et al., 2017). Diverse tree species composition enhances ecosystem resilience, providing niches for different organisms, and mitigating the risks associated with pests and diseases (FAO and UNEP, 2020). In addition to its ecological value, tree species composition is of key interest to the forest industry as different species are suitable for different end uses due to species-specific wood properties, such as fiber length and resistance to traction.

* Corresponding author.
E-mail addresses: raul.de.paula.pires@slu.se (R.P. Pires), christoffer.axelsson@slu.se (C. Axelsson), eva.lindberg@slu.se (E. Lindberg), henrik.persson@slu.se (H.J. Persson), kenneth.olofsson@slu.se (K. Olofsson), johan.holmgren@slu.se (J. Holmgren).

https://doi.org/10.1016/j.jag.2025.104607
Received 2 January 2025; Received in revised form 11 April 2025; Accepted 15 May 2025
Available online 21 May 2025

When it comes to mapping forest characteristics, LiDAR is one of the most commonly used tools (Coops et al., 2021; Nilsson et al., 2017). These sensors can be used to distinguish tree species based on their unique structural features, such as branch patterns and shapes (Holmgren and Persson, 2004; Terryn et al., 2020; Xi et al., 2020). For instance, Terryn et al. (2020) classified five species using branch patterns in Terrestrial Laser Scanning (TLS) data, achieving 80 % accuracy. Analogously, Qian et al. (2023) achieved 90.9 % accuracy using Aerial Laser Scanning (ALS) data to differentiate six species, leveraging vertical slices of point clouds to geometric shapes. Beyond structural features, multispectral LiDAR sensors offer additional spectral reflectance data from forest canopies (Takhtkeshha et al., 2024). The use of such systems for tree species identification has been widely explored in the scientific literature (Budei et al., 2018; Mielczarek et al., 2023; Yu et al., 2017), with some studies pointing out improvements in the retrieval of species-specific forest parameters (Kukkonen et al., 2019a, 2019b) and tree detection (Huo and Lindberg, 2020) when using multispectral LiDAR compared to other remote sensing data sources.

As remote sensing technologies advance, they generate increasingly complex datasets that require sophisticated analytical methods. For this reason, deep learning – in particular Convolutional Neural Networks (CNNs) – has gained prominence in analyzing remote sensing data due to its ability to analyze complex spectral and spatial patterns (Mäyrä et al., 2021; Sothe et al., 2020), with tree species classification being one of the most common tasks performed by CNNs in the fields of forestry and forest conservation (Kattenborn et al., 2021). For example, Wu et al. (2024) used a CNN for band selection in hyperspectral images, reducing data dimensionality for faster processing. Their FAST 3D-CNN P-Net classified nine tree species with 97 %-99 % accuracy across different areas. In the recent years, deep learning has been used for tree species classification in different types of remote sensing data, including RGB images (Carvalho et al., 2022; Liu et al., 2019; Onishi and Ise, 2021; Schiefer et al., 2020), satellite optical data (Bolyn et al., 2022; Hızal et al., 2024), multi- and hyperspectral imagery (Fricker et al., 2019; Ma et al., 2024; Sothe et al., 2020; Wang and Jiang, 2024; Xu et al., 2024), and LiDAR point clouds (Murray et al., 2024; Seidel et al., 2021).

Despite the success, different challenges arise when using such deep neural networks for forestry-related applications. One major bottleneck is the need for large datasets during model training, as acquiring high-quality, georeferenced annotated data is often time-consuming and expensive (Kattenborn et al., 2021). To address this challenge, strategies such as data augmentation (He et al., 2023; Oubara et al., 2022) and synthetic data generation are employed (Bryson et al., 2023; Xiang et al., 2023), increasing the training data diversity. Finally, emerging technologies such as UAV-borne laser scanners (UAVLS) and MLSs can be used to efficiently measure forest attributes, such as diameter at breast height (DBH) and stem volume, over large areas in short times (Hyyppä et al., 2022, 2020; Pires et al., 2022; Puliti et al., 2020), generating training data in sufficient amounts.

While such methods improve the availability of training data, complementary sources can further enhance model performance and reduce reliance on field surveys. A promising alternative is the use of spatially explicit Harvester Production Reports (HPRs) as training data for estimating forest attributes. HPRs are a by-product of mechanized harvesting, generated in large quantities as a part of routine forestry operations. These reports contain detailed georeferenced information on each harvested tree, such as taper and species, making them particularly valuable for precision forestry applications. When equipped with accurate positioning systems, HPRs provide the exact type of annotations required by precision forestry – at tree-level, accurate and spatially explicit. Thus, they represent a cost-effective way of enhancing remote sensing-based inventories, significantly reducing the resources needed for field data collection (Lindroos et al., 2015; Söderberg et al., 2021).

Despite their potential, HPRs remain underutilized in the context of deep learning applications for tree species classification. Leveraging HPRs as large-scale training data could significantly reduce reliance on field surveys while improving the accuracy of species classification models. In addition, such data source could enhance the estimation of continuous forest variables such as DBH and stem volume (Hauglin et al., 2018; Karjalainen et al., 2022; Maltamo et al., 2019; Noordermeer et al., 2023), and qualitative variables such as different kinds of forest damage (Hansen et al., 2023; Jamali et al., 2023).

Given the possibilities introduced by remote sensing, deep learning, and new training data sources, our main objective is to propose a method for automatically classifying tree species at single-tree level. For that, we use HPRs to automatically annotate ALS data at tree-level, and use the annotated data to train a tree species classification CNN. In addition, we investigate the proposed technique's performance under ALS datasets with different properties, namely different spectral and spatial resolutions.

2. Material and methods

2.1. Study area

The study area is located in central Sweden (59°46́N, 14°31́E – Fig. 1). Altogether, 17 stands were used in the study, with areas varying from 3.7 ha to 16.8 ha. The stands were selected according to their planned harvesting dates, between 2021 and 2022. On the harvested stands (Table 1) the dominant tree species are Norway spruce (*Picea abies* (L.) H. Karst.) – 79 %, Scots pine (*Pinus sylvestris* L.) – 11 %, and

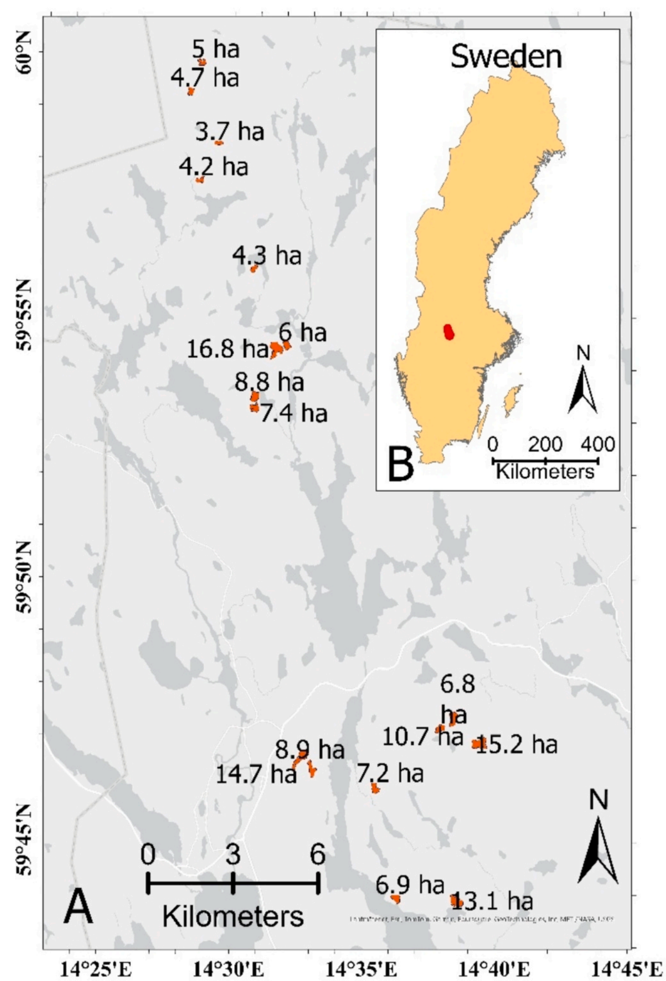

Fig. 1. (A) Map of the study area with the 17 harvested stands and their respective areas in hectares (ha). (B) Approximate location of the study area in Sweden, in red. (For interpretation of the references to color in this figure legend, the reader is referred to the web version of this article.)

Table 1
Forest areas' mean characteristics per tree species. DBH = Diameter at breast height in cm. SD = standard deviation.

Tree species	Mean DBH (± SD)	Basal area per hectare (m^2/ha)	Volume per hectare (m^3/ha)
Scots pine	25.5 (± 6.05)	6.02	59.7
Norway spruce	20.1 (± 7.99)	37.3	357
Deciduous	20.9 (± 7.96)	4.38	36.4
All species	**20.7 (± 7.99)**	**47.7**	**453**

Birch (*Betula* spp.) – 10 %.

2.2. Aerial laser scanning data

The stands were scanned in September 2021 using the Finnish Geospatial Institute's (FGI) dual-wavelength ALS system (Hakula et al., 2023). This system included two monochromatic LiDAR sensors: the Riegl miniVUX-1UAV (905 nm, NIR) and the Riegl VUX-1HA (1550 nm, SWIR), mounted on a helicopter flying 100 m above ground at 50 km/h. Due to technical issues, the system's third scanner (green wavelength) did not collect data, resulting in a dual-wavelength point cloud.

The point cloud was pre-processed and normalized using the LAStools software (Rapidlasso GmbH, Germany). Individual tree crowns were segmented using the Holmgren et al. (2022) algorithm, developed for boreal forests and achieving an F1 score of 0.86 for trees with DBH ≥ 10 cm (Pires et al., 2024). This method, previously used as the tree segmentation method for tree species classification studies (Axelsson et al., 2023; Persson et al., 2022), requires sample trees for crown density model creation. Accordingly, 122 trees were manually segmented to calibrate the model. The segmentation produced polygons representing individual tree crowns, with the highest point within each polygon identified as the treetop. To simulate different ALS systems, returns from the two sensors were separated post-segmentation, creating three datasets: mini-VUX (NIR), VUX (SWIR), and a dual-wavelength dataset combining both. Table 2 summarizes the characteristics of these datasets.

2.3. Harvester production reports

Altogether, 69,253 trees from 17 stands were harvested from November 2021 to October 2022 using cut-to-length (CTL) harvesters by John Deere (Moline, Illinois, United States) equipped with a positioning system. The positioning system consisted of two Global Navigation Satellite System (GNSS) receivers mounted on the harvester's cabin in order to establish its position and bearing. Built-in sensors enabled the recording of the boom angle and boom extension at the time of tree felling. However, the extension of the last part of the boom could not be recorded. Together, the integrated sensors for boom extension and angle and the GNSS on the harvester's cabin make it possible to calculate the position of each tree during felling. The positions of 34 stumps were taken with a RTK GNSS and used to assess the accuracy of the positions obtained with the harvester system. The distances between the stumps and harvester positions ranged from 0.1 to 2.1 m, with a mean of 0.38 m.

From the HPRs we extracted each tree's position, species, DBH, and the log lengths. Subsequently, the hprCM software (Skogforsk, 2022) was used to estimate each tree's volume and total height based on the information on the HPR. The HPR files stored four species classes, "Norway spruce", "Scots pine", "Birch", and "Other broadleaves". The "Birch" and "Other broadleaves" classes were combined into a single "Deciduous" class.

Table 2
Description of the aerial laser scanning (ALS) datasets used for tree species classification. PRR: Pulse Repetition Rate.

	ALS dataset		
	Mini-VUX (1)	**VUX (2)**	**Dual-wavelength (1 + 2)**
Sensor(s)	miniVUX-1UAV	VUX-1HA	miniVUX-1UAV (1) + VUX-1HA (2)
Footprint (cm) at 100 m from the target	16 x 5	5	16 x 5 (1) + 5 (2)
PRR (kHz)	100	1017	100 (1) + 1017 (2)
Scan speed (revolutions/s)	100	143	100 (1) + 143 (2)
Point density (points/m^2)	100	875	975 (1 + 2)
Wavelength (nm)	905	1550	905 (1) + 1550 (2)

2.4. Linking harvested trees to ALS data

Linking harvested trees to ALS segments was crucial for creating an annotated dataset with individual tree point clouds assigned to species classes. This was achieved by matching tree positions and heights between harvested trees and ALS-derived segments, using treetops from ALS segments as reference positions. For each harvested tree position, the product of horizontal distance (d) and height difference (dh) between the tree and neighboring treetops was calculated. If a treetop was within 1 m of the harvested tree, the closest treetop was linked to the harvested tree. If no treetops were within 1 m, the tree was linked to the treetop with the smallest $d \times dh$ value. Maximum allowed values were $d = 3.5$ m and $dh = 4$ m.

Segmented tree crowns, i.e. treetops, that were not linked to harvested trees were assumed to be trees that remained standing after the harvest or to be commission errors from individual tree segmentation. Harvested trees that were not linked to a tree crown were assumed omission errors from the individual tree segmentation.

Altogether, 45,516 tree positions were linked to an ALS-derived segment, representing 65.7 % of all harvested trees. Of those, 36,162 trees (79.4 %) were Norway spruces, 5,397 trees (11.9 %) Scots pine, and 3,957 (8.7 %) were deciduous trees. The proportion of trees linked to an ALS-derived segment increases with DBH (Fig. 2). In smaller DBH classes, e.g. from 5 – 10 cm, the majority of harvested trees were not linked to any ALS-derived segment. Conversely, this proportion decreases as the DBH increases, with the majority of trees with DBH ≥ 10 cm being linked to an ALS-derived segment.

2.5. Conversion of point clouds to 2D images

We used a CNN designed for 2D image classification – described further in section 2.6. Therefore, the individual tree point clouds were converted into images. The general workflow for this conversion involved transforming the individual tree point clouds into 2D images from four angles by rasterizing them in the X vs. Z plane at 45° intervals. At that stage, the pixel size was dynamically determined based on point density to ensure accurate representation of varying tree sizes and shapes, and the pixel values assigned according to the ALS dataset used, preserving relevant structural and spectral information. Finally, the pixel values were normalized and the images resized to a standard 160 × 320 pixels for CNN classification.

The rasterization was done in the X vs. Z plane, generating four 2D representations per tree by rotating the tree point cloud around the Z-axis at 45° intervals (0°, 45°, 90°, and 135°). It was performed independently for each ALS dataset and tree, producing variable image dimensions and pixel sizes tailored to tree size and dataset characteristics. Using fixed image dimension and pixel size for rasterizing the tree point clouds could lead to inaccuracies in their 2D representations. For instance, fixed image and pixel sizes could potentially cause trees to be cropped, if the number of pixels is not enough to cover their full extent, or blurred, if the pixel size is too large relative to the tree's size. By using variable pixel and image sizes, we were able to better represent the different tree sizes and shapes. This approach maintained the resolution of the original point cloud data, ensuring higher point density datasets were represented with higher-resolution images, while lower-density

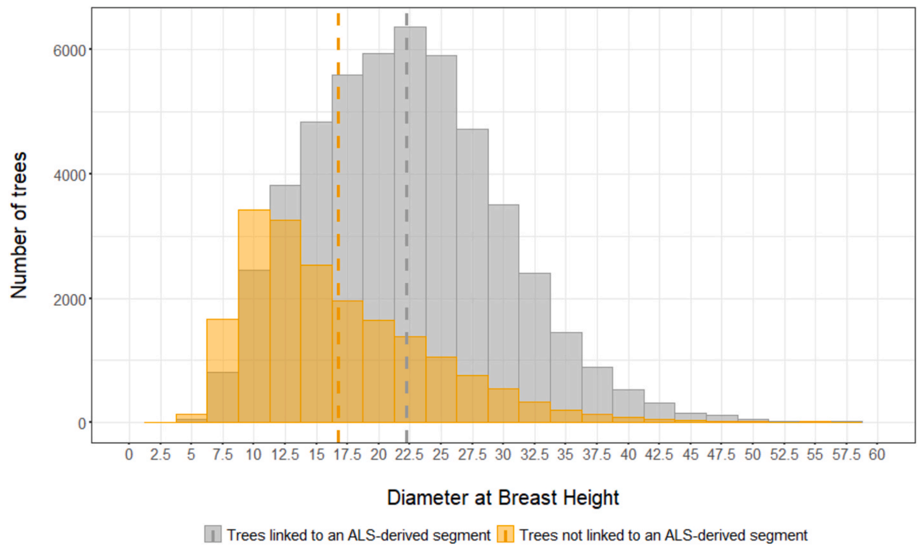

Fig. 2. Diameter at breast height (DBH) distribution of trees linked and not linked to an aerial laser scanning (ALS)-derived segment. The dashed lines represent the mean DBH of each category.

datasets retained appropriate detail levels.

Fig. 3 shows how point clouds of trees with different sizes were represented in two dimensions. Prior to rasterization, the extent of the point cloud for each rotation angle was used to define the area to be rasterized, ensuring accommodation of the entire point cloud within the raster frame. For each ALS dataset (i), tree (j) and rotation angle (a), the pixel size (ps) of the resulting 2D image was calculated according to formula 1. In this calculation, the pixel area was determined as the inverse of the point density in the X vs. Z direction post-rotation, representing the area a single point would occupy if all the returns in the point cloud were uniformly distributed within the raster frame.

$$ps_{ija} = \sqrt{(x_{ija} {}^{*} z_{ija})/n_{ij}} \quad (1)$$

where, n is the number of returns in the tree segment.

Once the raster frame and pixel size were established for each i, j and a, pixel values were assigned based on the ALS dataset used. In order to assess the implication of adding spectral information in the images used for classification, the pixel values in mini-VUX- and VUX-derived images was set as the number of returns within each pixel considering the full depth of a tree's point cloud. In other words, no intensity values in the two monochromatic datasets were used. The pixel values were normalized image-wise within the range of 0 to 255, with 0 indicating no points in the pixel and 255 corresponding to the 95th percentile of the pixel values pre-normalization. Pixels with values greater than or equal to the 95th percentile of pixel values were set as 255, resulting in grayscale images with 256 shades, ranging from white (0) to black (255).

In contrast, the images derived from dual-wavelength ALS data were created using an RGB false color composite combining NIR and SWIR. In each pixel, the red channel was assigned the mean intensity of the NIR points, green as the mean intensity of the SWIR points, and blue as the Normalized Near Infrared Index (NDII), calculated using NIR and SWIR according to formula 2. For these images, pixels lacking returns from either channel were assigned an NDII value of zero. Afterwards, the RGB values of each image were normalized to a range between 0 and 255, where 0 represented the absence of returns, and 255 indicated the highest mean intensity value before normalization.

$$NDII_k = \frac{nir_k - swir_i}{nir_i + swir_i} \quad (2)$$

where nir is the mean intensity of returns from the miniVUX-1UAV sensor, and $swir$ is the mean intensity of returns from the VUX-1HA sensor in pixel k.

Finally, all images were resized to the standard dimensions of 160 (width) by 320 (height) pixels.

2.6. *Tree species classification*

To ensure an even representation of each tree species class and mitigate potential bias towards over-represented classes, the dataset was balanced by reducing the number of instances in each class to match the smallest class. Thus, the number of trees in the Norway spruce and Scots pine classes was reduced to 3,957 trees to match the Deciduous class.

The dataset was visually inspected to create a "Noise" class for commission errors from tree segmentation. In this context, an image was classified as noise if we could not identify an obvious tree shape on the image within the dual-wavelength dataset. This step aimed to classify potential commission errors from the tree segmentation process as such, increasing the prediction accuracy for the tree species classes. If the images of a given segment were considered noise while inspecting the dual-wavelength dataset, they were sorted to the "Noise" class in all three ALS datasets. During this process, 228 trees were removed from the analysis due to being assigned the wrong species class, representing 0.5 % of all matched trees. These removals could be a result of faulty annotations by the harvester operator or errors in the matching procedure. Since species assignment is manually performed by the operator, human error is possible. Additionally, mismatches between harvester-derived and ALS-derived positions may have contributed to these removals. Altogether, 853 trees were sorted out from the other classes and allocated in the "Noise" class, resulting in 3772, 3559 and 3459 trees in the Pine, Spruce and Deciduous classes, respectively.

We used YOLOv8s-cls, a CNN from the YOLO family, for species classification due to its strong performance and user-friendly implementation in PyTorch (Jocher et al., 2023). The *YOLOv8s-cls* model, suitable for small-class problems, was trained for 15 epochs using default settings (Appendix A). Each tree was represented by four images from different views, resulting in nearly 14,000 images per class. Thirty percent of these were reserved for validation at each epoch's end. YOLO networks have demonstrated success in object detection tasks, including tree detection and segmentation (Straker et al., 2023) and wood surface knot detection (Fang et al., 2021), making YOLOv8 an ideal choice for this study.

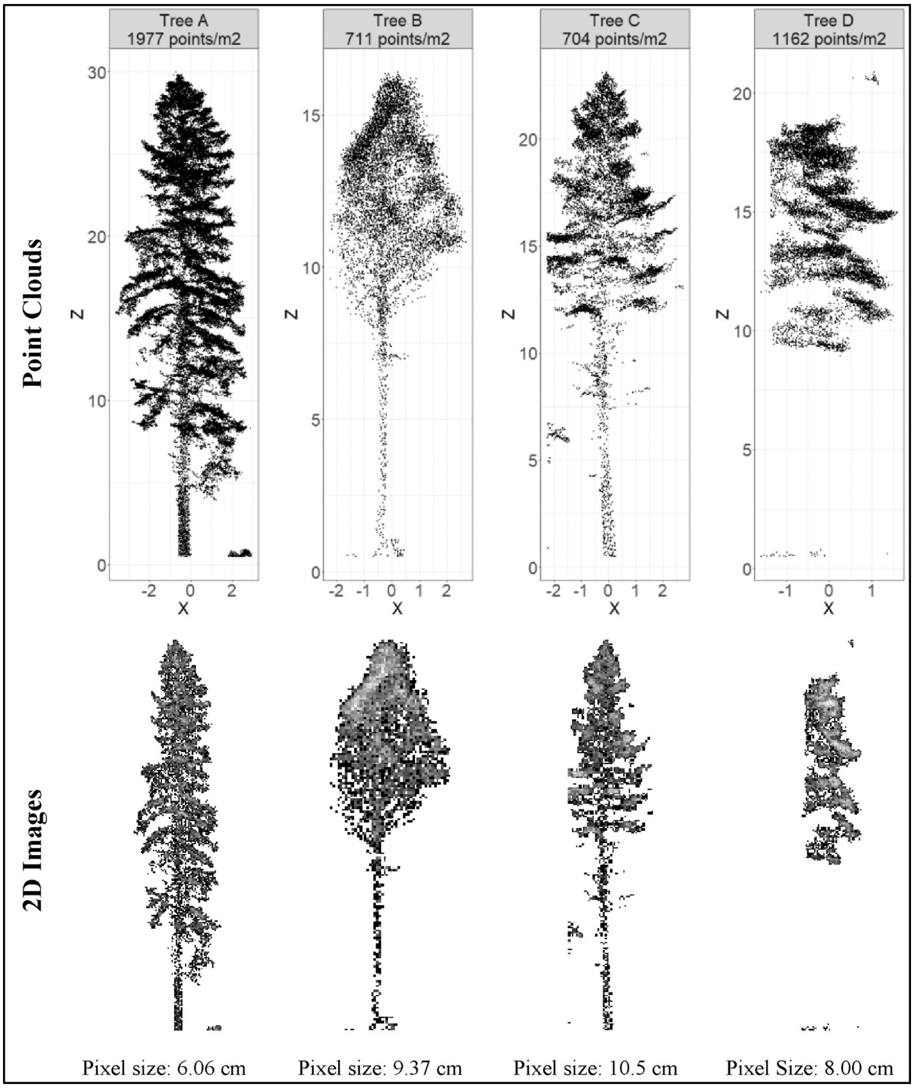

Fig. 3. Schematic representation of the rasterization of two trees with different point densities and sizes. Tree A: Norway spruce. Tree B: Deciduous tree. Tree C: Scots pine. Tree D: Pine tree under wrong segmentation, i.e. noise. The different shades of gray in the 2D image represent the number of points in each pixel. X and Z are in meters.

2.7. Accuracy Assessment

The tree species classification model's accuracy was assessed by comparing observed and predicted species for each tree. Due to the limited number of stands ($S = 17$), we opted for a leave-one-stand-out validation approach. For each stand s, the model was trained using data from all other stands ($S - s$) and applied to s. By doing so, we ensure that no trees from s are seen during the training process. This process was repeated S times, generating predictions for all stands while evaluating how the model is able to generalize when applied to different stands. During validation, the model predicted species independently for each tree projection, producing four probability vectors per ALS-derived segment. These vectors were averaged to create a single probability vector per segment, assigning the class with the highest probability to the segment. The leave-one-stand-out results are shown in a confusion matrix together with evaluation metrics such as user's and producer's accuracy (UA and PA as in formulas 3 and 4, respectively), the F1 score (formula 5), and overall accuracy (formula 6). Complementarily, the macroF1 represents the mean of the F1 score across all classes.

$$UA_C = TP_c/(TP_c + FP_C) \tag{3}$$

$$PA_C = TP_c/(TP_c + FN_C) \tag{4}$$

$$F1_C = 2 \bullet UA_C \bullet PA_C/(UA_C + PA_C) \tag{5}$$

$$OA = \frac{1}{N} \bullet \sum\nolimits_i^C TP_i \tag{6}$$

where TP is the number of true positives, FP are the false positives, and FN are the false negatives of class C. N represents the number of trees analyzed in this study.

3. Results

3.1. Conversion of point clouds to 2D images

Fig. 4 shows examples of 2D images generated from different ALS datasets for each classification category. Mini-VUX-based images had the lowest average resolution (27.6 cm pixel size, Table 3), often lacking finer details such as branch structures or visible trunks, which appeared blurred or absent. In contrast, images generated with VUX and dual-wavelength datasets had higher resolutions, averaging 10.1 cm and 9.52 cm pixel sizes, respectively, revealing finer details (Fig. 4, Table 3).

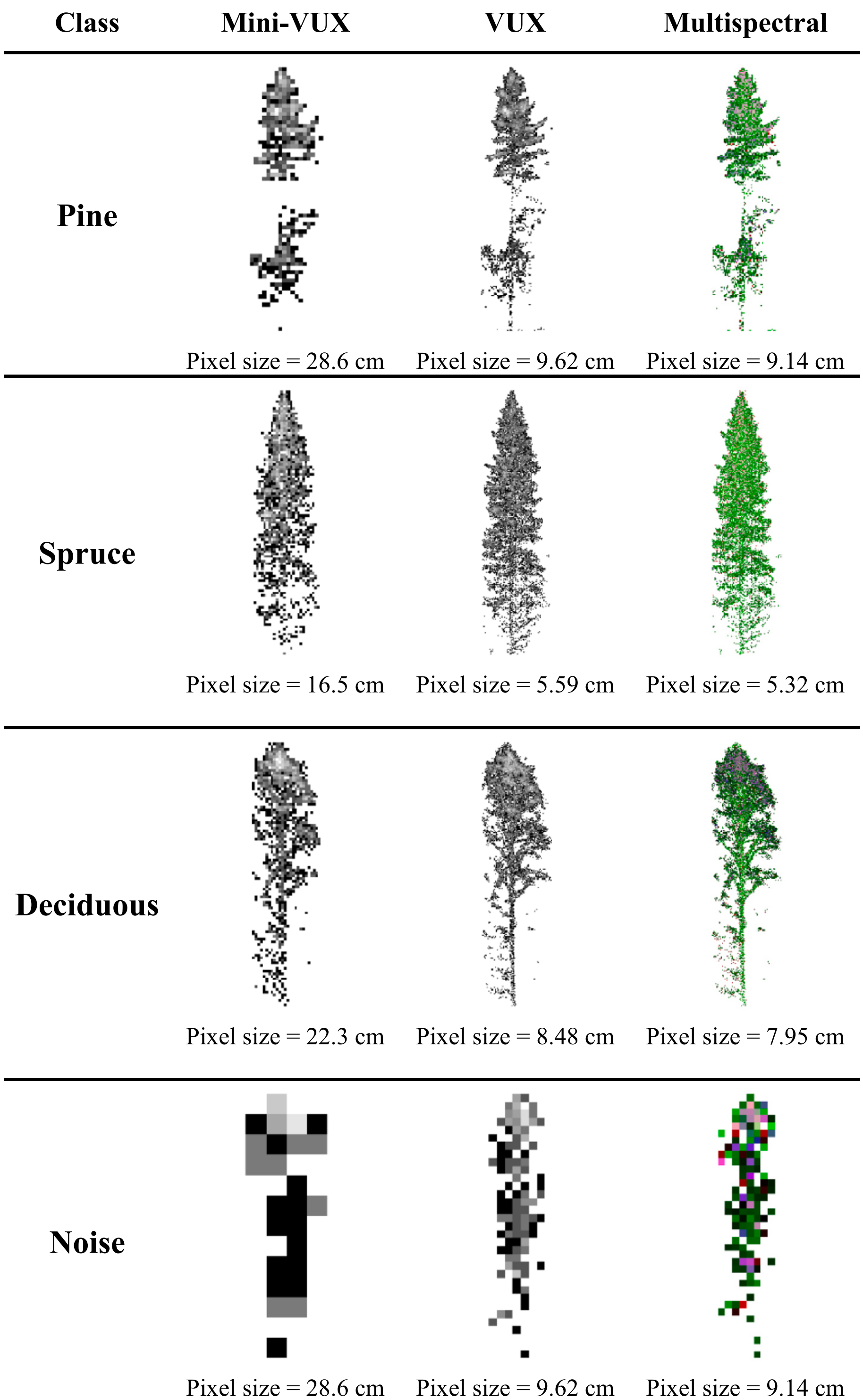

Fig. 4. Two dimensional representations of individual tree point clouds produced with different aerial laser scanning datasets.

In average, the Deciduous class had the largest pixel sizes of the tree species classes regardless of the dataset being used to generate the images (Table 3). This can be at least partially explained by the fact that the ALS data was collected in the beginning of the Autumn season, when the deciduous trees start shedding leaves, thus, intercepting less laser pulses then the other tree classes.

3.2. Tree species classification

Tables 4, 5 and 6 show the confusion matrixes and accuracy metrics for the classifications performed on the mini-VUX, VUX and dual-wavelength datasets, respectively. Fig. 5 shows an example of a a stand point cloud with all detected trees classified. The highest overall accuracies and macro-F1 obtained while using the dual-wavelength data for classification (Table 6), followed by the classification performed on the VUX data (Table 5). The classification done using the mini-VUX data showed the lowest F1 score for the three species classes and noise class, resulting in a macro F1 of 0.835 (Table 4).

The tree species classes showed the highest F1 score when using dual-wavelength images for classification, ranging from 0.923 to 0.942

Table 3
Average pixel size (cm) for the tree species classes and noise class (± standard deviation). Different letters in the last row denote statistically significant differences according to Student's *t*-test at a 95 % confidence level.

Class	Mini-VUX	VUX	Dual-wavelength
Pine	26.7 (± 5.88)	9.23 (± 2.1)	8.76 (± 1.98)
Spruce	27 (± 6.04)	9.61 (± 2.3)	9.11 (± 2.17)
Deciduous	27.5 (± 6.43)	10.5 (± 2.83)	9.88 (± 2.62)
Noise	38.9 (± 11.8)	16.4 (± 5.57)	15.4 (± 5.14)
All classes	**27.6 a (± 7.04)**	**10.1b (± 3.07)**	**9.52c (± 2.86)**

from Spruce to Decidous, resulting in a macro-F1 of 0.934 when not considering the Noise class. Analogously, when using VUX-based images, the F1 scores ranged from 0.914 (Spruce) to 0.937 (Pine), resulting in a macro-F1 of 0.926 when disregarding the Noise class. Finally, the lowest classification accuracy for the tree species classes was obtained while using mini-VUX-based images (Table 4). With this dataset, the F1 scores ranged from 0.84 for the Deciduous class to 0.876 for the Spruce class, with a macro F1 of 0.861 when considering only the tree species classes. The F1 scores were the lowest for the Noise class regardless of the ALS dataset used for modelling and inference. For this class, the F1 scores were 0.756, 0.798 and 0.783 when using the mini-VUX, VUX and dual-wavelength datasets, respectively.

Even though improvements in the classification accuracy were observed across all classes when using ALS datasets with higher spatial and spectral resolutions, some classes benefited more from the higher resolution datasets than others. For example, when using the mini-VUX dataset for classification, the Deciduous class exhibited the lowest accuracy among the tree species classes (F1 = 0.840). However, this class showed intermediate classification accuracy when using VUX (F1 = 0.928) and the highest accuracy of all species groups when using the dual-wavelength dataset (F1 = 0.942), representing more an improvement of 12.1 % on the F1 score. In contrast, the Pine class' F1 score improved 8.07 % and Spruce class' 5.37 % when comparing the classification done using mini-VUX and dual-wavelength data.

We also examined the relationship between classification accuracy and stand conditions such as tree density, basal area and species mixture measures. However, no meaningful correlation was observed ($R^2 < 0.1$), suggesting that classification performance was not strongly influenced by these factors.

4. Discussion

4.1. Using HPRs for tree species classification

In this study, we used harvester production reports to automatically annotate three ALS datasets, with different spatial and spectral resolutions. With this approach, 45,516 ALS-derived individual tree segments were labeled with tree species information by matching spatially explicit information from HPRs to the ALS-derived single tree positions, representing 65.7 % of the trees harvested in the study area. This proportions align with other studies reporting rates form from 42.8 % (Mäyrä et al., 2021) to 69.3 % (Hamraz et al., 2019).

Despite links being established across all DBH classes, many harvested trees remained unlinked (Fig. 2). In this study, we could not determine the exact reasons for this, as not all trees in the study area were harvested. Common forestry practices, such as leaving shelter wood or partially harvesting stands, may explain some missing links. Additionally, the tree segmentation method used has shown reduced detection rates for smaller trees (Holmgren et al., 2022; Pires et al., 2024), suggesting that improved detection of small trees in ALS data could enhance linking rates.

This is a known limitation of ALS-based tree detection and segmentation, as smaller individuals in the understory that are often occluded. In this study, many of the harvested trees that were not linked to ALS-derived segments fell within lower DBH classes (Fig. 2), suggesting

Table 4
Confusion matrix of predictions made using the mini-VUX-based images. OA = Overall accuracy.

		Observed Species				User's accuracy	F1 score
		Pine	Spruce	Deciduous	Noise		
Predicted Species	Pine	3190	137	292	17	87.7 %	0.867
	Spruce	245	3233	206	97	89.8 %	0.876
	Deciduous	257	158	2886	114	84.5 %	0.840
	Noise	30	71	75	625	78 %	0.756
Producer's accuracy		85.7 %	87.6 %	83.4 %	73.3 %	**OA = 85.4 %**	**macroF1 = 0.835**

Table 5
Confusion matrix of predictions made using the VUX-based images. OA = Overall accuracy.

		Observed Species				User's accuracy	F1 score
		Pine	Spruce	Deciduous	Noise		
Predicted Species	Pine	3409	85	57	5	95.9 %	0.937
	Spruce	203	3362	109	80	89.6 %	0.914
	Deciduous	94	76	3207	85	92.6 %	0.928
	Noise	16	76	86	686	79.4 %	0.798
Producer's accuracy		91.6 %	93.4 %	92.7 %	80.1 %	**OA = 91.6 %**	**macroF1 = 0.894**

Table 6
Confusion matrix of predictions made using the dual-wavelength images. OA = Overall accuracy.

		Observed Species				User's accuracy	F1 score
		Pine	Spruce	Deciduous	Noise		
Predicted Species	Pine	3455	103	87	9	94.6 %	0.937
	Spruce	198	3392	60	100	90.4 %	0.923
	Deciduous	45	43	3242	97	94.6 %	0.942
	Noise	24	61	70	650	80.8 %	0.783
Producer's accuracy		92.8 %	94.2 %	93.7 %	75.9 %	**OA = 92.3 %**	**macroF1 = 0.896**

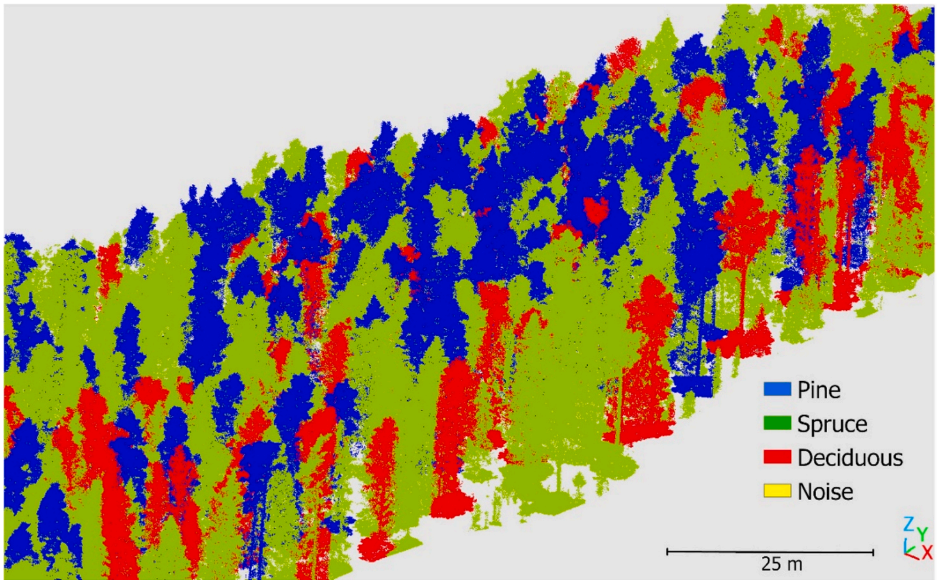

Fig. 5. Example of a stand's point cloud after tree species classification under the proposed methodology.

that suppressed trees were underrepresented in the annotated dataset. The omission of these trees introduces a potential source of bias, as the classification model is predominantly trained on dominant and co-dominant individuals. Similar issues have been reported in previous studies, which found that small or suppressed trees are frequently missing from ALS-derived individual tree-level inventories (Xu et al., 2014a, 2014b).

To mitigate this limitation, future research could explore strategies such as targeted data augmentation for suppressed trees to increase their representation during model training. Alternatively, the integration of complementary datasets, such as benchmark datasets (Puliti et al., 2023b) from structurally heterogeneous stands or synthetic point clouds that simulate occluded understory trees, may help models learn features of suppressed individuals more effectively. These approaches can provide a partial workaround to underrepresentation by enriching the training data, even when direct segmentation of suppressed trees is not feasible.

Nevertheless, the annotation effort required in this study was significantly lower compared to manual interpretation of LiDAR point clouds or traditional field data collection. Annotation remains a major challenge for training deep learning models, which often require a large number of annotated instances (Hamedianfar et al., 2022). Hence, HPRs can simplify this process and provide additional tree size attributes such as DBH, height, and volume, which are important for various modeling tasks (Hauglin et al., 2018; Karjalainen et al., 2022; Maltamo et al., 2019; Noordermeer et al., 2023).

4.2. Conversion of point clouds to 2D images

Conversion of three-dimensional point clouds to two-dimensional representations is a common approach to detection, segmentation and classification problems when using deep learning on point clouds (Kattenborn et al., 2021), either by using a single- or multi-view 2D-CNNs (Zhang et al., 2023). With such approach, users are able to apply well-established deep learning architectures and frameworks used for 2D data processing also on data originally acquired in three dimensions. For instance, Persson et al. (2022) converted individual tree ALS point clouds to 2D images from different views in order to use a CNN for tree species classification. Puliti et al. (2023a) used UAVLS data to create 2D vertical projections of Norway spruce trees' and train a whorl detector using the YOLOv5 framework (Jocher, 2020). In addition, Hamraz et al. (2019) estimated the conifer and deciduous proportions at area-level using either a LiDAR-based Digital Surface Model (DSM) or projections of the LiDAR point cloud from different viewpoints. Moreover, Straker et al. (2023) performed instance segmentation of individual trees using YOLOv5 and UAVLS-based Canopy Height Models (CHM).

When it comes to tree species classification at tree-level, Briechle et al. (2021) converted UAVLS point clouds with approximately 53 points/m^2 to 2D side view projections. In their study, the pixel size was set to 10 cm and the image size was set to accommodate the largest tree in the dataset without cropping it, which resulted in a considerable loss of detail when projecting smaller trees. In a simpler conversion approach, Hell et al. (2022) generated side-view images of tree-level ALS point clouds (with approximately 80 points/m^2) by producing scatterplots with the point locations in the vertical direction. These scatterplots were written as 150 x 150 pixel images and used as input for a CNN. However, in order to avoid smaller trees being represented with more details than bigger trees, only adult forest trees were included in the analysis.

We were able to avoid shortcomings related to projecting point clouds with different dimensions by using variable pixel sizes and image dimensions while projecting the ALS-derived segments into 2D images and, later, resizing all the images to the standard 320x160 pixel resolution to be used by the CNN. This allowed us to use the state-of-the-art YOLOv8 framework for classification (Jocher et al., 2023), which is known for its user friendliness, speed and accuracy. In addition, the memory required to store 2D images of 320x160 pixels was considerably smaller than the one that would be required if storing point clouds, especially when considering that the average point density was nearly 1000 points/m^2.

4.3. Tree species classification using ALS data

Tree species classification accuracies varied with the ALS dataset used. Using the dual-wavelength dataset (NIR and SWIR returns), the macro-F1 score was 0.896, and overall accuracy (OA) reached 92.3 %. Similar performance was achieved with VUX dataset images (macro-F1 = 0.894, OA = 91.6 %), while mini-VUX dataset predictions yielded lower accuracy (macro-F1 = 0.835, OA = 85.4 %). The VUX dataset's higher spatial resolution resulted in a 6.2 % OA increase over mini-VUX, with the macro-F1 rising from 0.835 to 0.894. Conversely, using dual-wavelength data only slightly improved OA (from 91.6 % to 92.3 %) and macro-F1 (from 0.892 to 0.893). This discrepancy may be attributed to differences in point density and laser beam footprint: the VUX dataset had footprints of nearly 20 cm2 at 100 m, while mini-VUX footprints were approximately 63 cm2, reducing visibility of smaller features like fine branches in mini-VUX-derived images. In other words, similar tree species classification accuracies were obtained when using the monochromatic VUX dataset and the dual-wavelength dataset under the proposed methodology. This result can be at least partially explained by the fact that CNNs such as the one used in this study are designed to learn from local patterns in images (Hamedianfar et al., 2022; Kattenborn et al., 2021), such as the different tree shapes and branches. Consequently, when classifying Pine, Spruce, Deciduous, and Noise, which differ substantially in shape (Figs. 3 and 4), point density and small footprint scanning might have been more determinant than spectral information.

The observed differences in classification accuracy across tree species highlight the role of the tree crowns' structural complexity and spectral information in species differentiation (Nauber et al., 2024; Qian et al., 2023; Terryn et al., 2020). The Deciduous class, which exhibit more variable and heterogeneous crown structures, benefited the most from the VUX and dual-wavelength datasets likely due to the increased spatial resolution capturing finer details necessary for accurate classification. The further improvement observed with dual-wavelength data suggests that spectral information enhances species differentiation by capturing variations in foliage properties (Shi et al., 2018a, 2018b). In contrast, Pine and Spruce classes showed smaller accuracy gains, indicating that their more uniform crowns are more easily distinguishable even with lower-resolution datasets. However, this study is limited to a single geographical region and a few species groups. Hence, it was not possible to access how the spectral information from dual-wavelength LiDAR point cloud would influence tree species classification accuracy when classifying more species groups or trees from different biomes.

Yet, the classification accuracies obtained are in-line with other studies that have attempted tree species classification using either single- or multi-wavelength LiDAR data in similar forest types. For example, Axelsson et al. (2023) used a dual-wavelength ALS system (532 nm and 1064 nm) and k-nn imputation to classify Pine, Spruce, and Deciduous trees, obtaining OA of 91.1 % and macro-F1 of 0.861. Hakula et al. (2023) used multispectral ALS (532 nm, 905 nm and 1550 nm) and random forest for classifying similar species, obtaining OA of 90.8 % and macro-F1 of 0.901.

Regarding deep learning approaches, our CNN-based method using 2D projections aligns with similar methodologies that have shown high classification accuracy. Mäyrä et al. (2021) used 3D-CNNs with ALS and hyperspectral images, obtaining OA of 87 % and macro F1 equal to 0.86 for four species groups. Briechle et al. (2021) achieved high accuracy (OA = 96.1 % and macro–F1 = 0.96) when combining LiDAR-derived side views and multispectral images in a 2D-CNN but noted reduced accuracy using LiDAR alone (OA = 80.4 %, macro-F1 = 0.8). Finally, Hell et al. (2022), used side-view 2D projections of individual trees from LiDAR data to classify seven tree species in temperate forests, reaching an overall accuracy of 87 %.

In addition to using 2D images or point cloud projections, authors have used deep learning models for classification directly in 3D point clouds. For example, Liu et al. (2022) benchmarked six point cloud-based deep learning models to classify eight species classes in dense MLS point clouds, achieving F1 scores ranging from 0.718 to 0.996. Murray et al. (2024) obtained weighted F1 scores of 0.63 when classifying the leading tree species and 0.85 when differentiating between coniferous- and broadleaf-dominated forest plots by using point-based deep learning in ALS data with approximately 40 points/m^2. These studies highlight that deep learning approaches are highly effective for tree species classification, particularly when incorporating high-resolution data. While point cloud-based methods provide a more direct way of processing LiDAR data, they typically require higher computational power. Our approach, using 2D projections with CNNs provides a simpler alternative while maintaining competitive accuracy.

Regardless of the architecture or type of model chosen, the automatic annotation used in our analysis can significantly affect how deep learning models are trained by eliminating the bottleneck of training data collection and manual annotation, enabling more scalable and efficient model development. By leveraging HPRs for species labeling, this approach enhances the feasibility of large-scale tree species classification efforts and opens new possibilities for integrating operational forestry data into remote sensing applications.

The classification method's performance could be improved by refining tree segmentation techniques, particularly for smaller trees. This could lead to an increase in the proportion of linked trees and improve dataset completeness. Apart from tree species classification, harvester data could be valuable for estimating other forest attributes, such as tree health, wood quality, or growth rates, by leveraging the recorded DBH, height, and volume measurements and expanding the usage of harvester data in remote sensing-based analyses.

5. Conclusion

This study proposes a method for automatically classifying tree species at the single-tree level using ALS data, deep learning, and harvester production reports. By using the HPRs to annotate ALS data, we effectively trained a tree species classification CNN, achieving macroF1 scores ranging from 0.835 to 0.896. The results indicate that spatially explicit HPRs are a promising data source for tree species identification at the single-tree level. Moreover, the best classification performance was achieved when using the dual-wavelength ALS dataset under the proposed methodology, closely followed by VUX dataset. The worst classification performance was obtained when using the mini-VUX data for classification. Future research should focus on implementing similar methodologies for diverse species groups, such as different deciduous trees.

CRediT authorship contribution statement

Raul de Paula Pires: Writing – original draft, Visualization, Validation, Methodology, Formal analysis, Conceptualization. **Christoffer Axelsson:** Writing – review & editing, Software, Methodology. **Eva Lindberg:** Writing – review & editing, Supervision, Resources, Methodology, Conceptualization. **Henrik Jan Persson:** Writing – review & editing, Supervision, Conceptualization. **Kenneth Olofsson:** Writing – review & editing, Methodology, Conceptualization. **Johan Holmgren:** Writing – review & editing, Supervision, Software, Resources, Methodology, Funding acquisition, Conceptualization.

Declaration of competing interest

The authors declare that they have no known competing financial interests or personal relationships that could have appeared to influence the work reported in this paper.

Acknowledgements

This study was financed by Stora Enso, and the Kempe foundations through the project "Estimating Forest Resources and Quality-related Attributes Using Automated Methods and Technologies" which was part of the Tandem Forest values research program (Grant Number TF 2019-0064). In addition, funding was provided by the Hildur and Sven Wingquist foundation for forest science research though the project "Multi sensor remote sensing for improved information in forest management planning" (Grant number 17/18-2 / 107-5 SOJOH) and the Bo Rydin Foundation for Scientific Research thought the project "F 06/21 Multi-phase inventory of forest using high-resolution laser scanning". Finally, co-financing was provided by the Swedish Foundation for Strategic Environmental Research with the research program Mistra Digital Forest (DIA 2017/14 #6). The authors wish to thank Skogforsk and Stora Enso for performing the harvester data collection and providing the harvester data logs. Finally, the authors would also like to thank the Finnish Geospatial Institute for the collection of aerial laser scanning data.

Author contributions

Raul de P. Pires: Conceptualization, Methodology, Validation, Formal analysis, Writing – Original Draft, and Visualization. **Christoffer Axelsson**: Methodology, Software, Writing - Review & Editing. **Eva Lindberg**: Conceptualization, Methodology, Resources, Writing - Review & Editing, and Supervision. **Henrik J. Person**: Conceptualization, Methodology, Writing - Review & Editing, and Supervision. **Kenneth Olofsson**: Conceptualization, Methodology, Writing - Review & Editing, and Supervision. **Johan Holmgren**: Conceptualization, Methodology, Software, Resources, Writing - Review & Editing, Supervision, and Funding acquisition.

Appendix A. Yolov8s-cls hyperparameters

task: classify; **mode**: train; **model**: yolov8s-cls.yaml; **epochs**: 15; **patience**: 3; **batch**: 16; **imgsz**: 320; **save**: true; save_**period**: −1; **cache**: true; **device**: 0; **workers**: 8; **exist_ok**: false; **pretrained**: false; **optimizer**: auto; **verbose**: true; **seed**: 27; **deterministic**: true; **single_cls**: false; **rect**: true; **cos_lr**: false; **close_mosaic**: 10; **resume**: false; **amp**: false; **fraction**: 1.0; **profile**: false; **freeze**: null; **overlap_mask**: truemask_ratio: 4; **dropout**: 0.25; **val**: true; **split**: val; **save_json**: false; **save_hybrid**: false; **conf**: null; **iou**: 0.7; **max_det**: 300; **half**: false; **dnn**: false; **plots**: true; **source**: null; **show**: false; **save_txt**: false; **save_conf**: false; **save_crop**: false; **show_labels**: true; **show_conf**: true; **vid_stride**: 1; **stream_buffer**: false; **line_width**: null; **visualize**: false; **augment**: false; **agnostic_nms**: false; **classes**: null; **retina_masks**: false; **boxes**: true; **format**: torchscript; **keras**: false; **optimize**: false; **int8**: false; **dynamic**: false; **simplify**: false; **opset**: null; **workspace**: 4; **nms**: false; **lr0**: 0.01; **lrf**: 0.01; **momentum**: 0.937; **weight_decay**: 0.0005; **warmup_epochs**: 3.0; **warmup_momentum**: 0.8; **warmup_bias_lr**: 0.1; **box**: 7.5; **cls**: 0.5; **dfl**: 1.5; **pose**: 12.0; **kobj**: 1.0; **label_smoothing**: 0.0; **nbs**: 64; **hsv_h**: 0.015; **hsv_s**: 0.7; **hsv_v**: 0.4; **degrees**: 0.0; **translate**: 0.1; **scale**: 0.5; **shear**: 0.0; **perspective**: 0.0; **flipud**: 0.0; **fliplr**: 0.5; **mosaic**: 1.0; **mixup**: 0.0; **copy_paste**: 0.0; **cfg**: null; **tracker**: botsort.yaml.

Data availability

The authors do not have permission to share data.

References

Axelsson, C.R., Lindberg, E., Persson, H.J., Holmgren, J., 2023. The use of dual-wavelength airborne laser scanning for estimating tree species composition and species-specific stem volumes in a boreal forest. Int. J. Appl. Earth Obs. Geoinf. 118, 103251. https://doi.org/10.1016/j.jag.2023.103251.

Bolyn, C., Lejeune, P., Michez, A., Latte, N., 2022. Mapping tree species proportions from satellite imagery using spectral–spatial deep learning. Remote Sens. Environ. 280, 113205. https://doi.org/10.1016/j.rse.2022.113205.

Briechle, S., Krzystek, P., Vosselman, G., 2021. Silvi-Net – A dual-CNN approach for combined classification of tree species and standing dead trees from remote sensing data. Int. J. Appl. Earth Obs. Geoinf. 98, 102292. https://doi.org/10.1016/j.jag.2020.102292.

Bryson, M., Wang, F., Allworth, J., 2023. Using Synthetic Tree Data in Deep Learning-Based Tree Segmentation Using LiDAR Point Clouds. Remote Sens. 15. https://doi.org/10.3390/rs15092380.

Budei, B.C., St-Onge, B., Hopkinson, C., Audet, F.A., 2018. Identifying the genus or species of individual trees using a three-wavelength airborne lidar system. Remote Sens. Environ. 204, 632–647. https://doi.org/10.1016/j.rse.2017.09.037.

Carvalho, M. de A., Marcato, J., Martins, J.A.C., Zamboni, P., Costa, C.S., Siqueira, H.L., Araújo, M.S., Gonçalves, D.N., Furuya, D.E.G., Osco, L.P., Ramos, A.P.M., Li, J., de Castro, A.A., Gonçalves, W.N., 2022. A deep learning-based mobile application for tree species mapping in RGB images. Int. J. Appl. Earth Obs. Geoinf. 114, 103045. DOI: 10.1016/j.jag.2022.103045.

Coops, N.C., Tompalski, P., Goodbody, T.R.H., Queinnec, M., Luther, J.E., Bolton, D.K., White, J.C., Wulder, M.A., van Lier, O.R., Hermosilla, T., 2021. Modelling lidar-derived estimates of forest attributes over space and time: A review of approaches and future trends. Remote Sens. Environ. 260, 112477. https://doi.org/10.1016/j.rse.2021.112477.

FAO, UNEP, 2020. The State of the World's Forests 2020. Forests, biodiversity and people. Rome. DOI: 10.4060/ca8642en.

Fardusi, M.J., Chianucci, F., Barbati, A., 2017. Concept to practices of geospatial information tools to assist forest management & planning under precision forestry framework: A review. Ann. Silvic. Res. 41, 3–14. https://doi.org/10.12899/asr-1354.

Fassnacht, F.E., Latifi, H., Stereńczak, K., Modzelewska, A., Lefsky, M., Waser, L.T., Straub, C., Ghosh, A., 2016. Review of studies on tree species classification from remotely sensed data. Remote Sens. Environ. 186, 64–87. https://doi.org/10.1016/j.rse.2016.08.013.

Fassnacht, F.E., White, J.C., Wulder, M.A., Næsset, E., 2024. Remote sensing in forestry: current challenges, considerations and directions. Forestry 97, 11–37. https://doi.org/10.1093/forestry/cpad024.

Fricker, G.A., Ventura, J.D., Wolf, J.A., North, M.P., Davis, F.W., Franklin, J., 2019. A convolutional neural network classifier identifies tree species in mixed-conifer forest from hyperspectral imagery. Remote Sens. 11. https://doi.org/10.3390/rs11192326.

Hakula, A., Ruoppa, L., Lehtomäki, M., Yu, X., Kukko, A., Kaartinen, H., Taher, J., Matikainen, L., Hyyppä, E., Luoma, V., Holopainen, M., Kankare, V., Hyyppä, J., 2023. Individual tree segmentation and species classification using high-density close-range multispectral laser scanning data. ISPRS Open J. Photogramm. Remote Sens. 9. https://doi.org/10.1016/j.ophoto.2023.100039.

Hamedianfar, A., Mohamedou, C., Kangas, A., Vauhkonen, J., 2022. Deep learning for forest inventory and planning: a critical review on the remote sensing approaches so far and prospects for further applications. For. an Int. J. for. Res. 1–15. https://doi.org/10.1093/forestry/cpac002.

Hamraz, H., Jacobs, N.B., Contreras, M.A., Clark, C.H., 2019. Deep learning for conifer/deciduous classification of airborne LiDAR 3D point clouds representing individual trees. ISPRS J. Photogramm. Remote Sens. 158, 219–230. https://doi.org/10.1016/j.isprsjprs.2019.10.011.

Hansen, E., Wold, J., Dalponte, M., Gobakken, T., Noordermeer, L., Ørka, H.O., 2023. Estimation of the occurrence, severity, and volume of heartwood rot using airborne laser scanning and optical satellite data. Eur. J. Remote Sens. 56. https://doi.org/10.1080/22797254.2023.2229501.

Hauglin, M., Hansen, E., Sørngård, E., Næsset, E., Gobakken, T., 2018. Utilizing accurately positioned harvester data: Modelling forest volume with airborne laser scanning. Can. J. for. Res. 48, 913–922. https://doi.org/10.1139/cjfr-2017-0467.

He, Y., Jia, K., Wei, Z., 2023. Improvements in Forest Segmentation Accuracy Using a New Deep Learning Architecture and Data Augmentation Technique. Remote Sens. 15. https://doi.org/10.3390/rs15092412.

Hell, M., Brandmeier, M., Briechle, S., Krzystek, P., 2022. Classification of Tree Species and Standing Dead Trees with Lidar Point Clouds Using Two Deep Neural Networks: PointCNN and 3DmFV-Net. PFG -. J. Photogramm. Remote Sens. Geoinf. Sci. 90, 103–121. https://doi.org/10.1007/s41064-022-00200-4.

Hızal, C., Gülsu, G., Akgün, H.Y., Kulavuz, B., Bakırman, T., Aydın, A., Bayram, B., 2024. Forest Semantic Segmentation Based on Deep Learning Using Sentinel-2 Images. Int. Arch. Photogramm. Remote Sens. Spat. Inf. Sci. - ISPRS Arch. 48, 229–236. https://doi.org/10.5194/isprs-archives-XLVIII-4-W9-2024-229-2024.

Holmgren, J., Lindberg, E., Olofsson, K., Persson, H.J., 2022. Tree crown segmentation in three dimensions using density models derived from airborne laser scanning. Int. J. Remote Sens. 43, 299–329. https://doi.org/10.1080/01431161.2021.2018149.

Holmgren, J., Persson, Å., 2004. Identifying species of individual trees using airborne laser scanner. Remote Sens. Environ. 90, 415–423. https://doi.org/10.1016/S0034-4257(03)00140-8.

Holopainen, M., Vastaranta, M., Hyyppä, J., 2014. Outlook for the next generation's precision forestry in Finland. Forests 5, 1682–1694. https://doi.org/10.3390/f5071682.

Huo, L., Lindberg, E., 2020. Individual tree detection using template matching of multiple rasters derived from multispectral airborne laser scanning data. Int. J. Remote Sens. 41, 9525–9544. https://doi.org/10.1080/01431161.2020.1800127.

Hyyppä, E., Hyyppä, J., Hakala, T., Kukko, A., Wulder, M.A., White, J.C., Pyörälä, J., Yu, X., Wang, Y., Virtanen, J.P., Pohjavirta, O., Liang, X., Holopainen, M., Kaartinen, H., 2020. Under-canopy UAV laser scanning for accurate forest field measurements. ISPRS J. Photogramm. Remote Sens. 164, 41–60. https://doi.org/10.1016/j.isprsjprs.2020.03.021.

Hyyppä, E., Kukko, A., Kaartinen, H., Yu, X., Muhojoki, J., Hakala, T., Hyyppä, J., 2022. Direct and automatic measurements of stem curve and volume using a high-resolution airborne laser scanning system. Sci. Remote Sens. 5, 100050. https://doi.org/10.1016/j.srs.2022.100050.

Jamali, S., Olsson, P.O., Ghorbanian, A., Müller, M., 2023. Examining the potential for early detection of spruce bark beetle attacks using multi-temporal Sentinel-2 and harvester data. ISPRS J. Photogramm. Remote Sens. 205, 352–366. https://doi.org/10.1016/j.isprsjprs.2023.10.013.

Jocher, G., 2020. YOLOv5 by Ultralytics (Version 7.0). DOI: 10.5281/zenodo.3908559.

Jocher, G., Chaurasia, A., Qiu, J., 2023. Ultralytics YOLO (Version 8.0.0).

Karjalainen, T., Mehtätalo, L., Packalén, P., Malinen, J., Næsset, E., Gobakken, T., Maltamo, M., 2022. In-situ calibration of stand level merchantable and sawlog volumes using cut-to-length harvester measurements and airborne laser scanning data. For. an Int. J. for. Res. 95, 105–117. https://doi.org/10.1093/forestry/cpab031.

Kattenborn, T., Leitloff, J., Schiefer, F., Hinz, S., 2021. Review on Convolutional Neural Networks (CNN) in vegetation remote sensing. ISPRS J. Photogramm. Remote Sens. 173, 24–49. https://doi.org/10.1016/j.isprsjprs.2020.12.010.

Kukkonen, M., Maltamo, M., Korhonen, L., Packalen, P., 2019a. Comparison of multispectral airborne laser scanning and stereo matching of aerial images as a single sensor solution to forest inventories by tree species. Remote Sens. Environ. 231, 111208. https://doi.org/10.1016/j.rse.2019.05.027.

Kukkonen, M., Maltamo, M., Korhonen, L., Packalen, P., 2019b. Multispectral Airborne LiDAR Data in the Prediction of Boreal Tree Species Composition. IEEE Trans. Geosci. Remote Sens. 57, 3462–3471. https://doi.org/10.1109/TGRS.2018.2885057.

Lindroos, O., Ringdahl, O., Hera, P.L., Hohnloser, P., Hellström, T., 2015. Estimating the position of the harvester head – A key step towards the precision forestry of the future? Croat. J. for. Eng. 36, 147–164.

Liu, B., Huang, H., Su, Y., Chen, S., Li, Z., Chen, E., Tian, X., 2022. Tree Species Classification Using Ground-Based LiDAR Data by Various Point Cloud Deep Learning Methods. Remote Sens. 14. https://doi.org/10.3390/rs14225733.

Liu, J., Wang, X., Wang, T., 2019. Classification of tree species and stock volume estimation in ground forest images using Deep Learning. Comput. Electron. Agric. 166, 105012. https://doi.org/10.1016/j.compag.2019.105012.

Ma, Y., Zhao, Y., Im, J., Zhao, Y., Zhen, Z., 2024. A deep-learning-based tree species classification for natural secondary forests using unmanned aerial vehicle hyperspectral images and LiDAR. Ecol. Indic. 159. https://doi.org/10.1016/j.ecolind.2024.111608.

Maltamo, M., Hauglin, M., Næsset, E., Gobakken, T., 2019. Estimating stand level stem diameter distribution utilizing harvester data and airborne laser scanning. Silva Fenn. 53, 1–19. https://doi.org/10.14214/sf.10075.

Mäyrä, J., Keski-Saari, S., Kivinen, S., Tanhuanpää, T., Hurskainen, P., Kullberg, P., Poikolainen, L., Viinikka, A., Tuominen, S., Kumpula, T., Vihervaara, P., 2021. Tree species classification from airborne hyperspectral and LiDAR data using 3D convolutional neural networks. Remote Sens. Environ. 256. https://doi.org/10.1016/j.rse.2021.112322.

Mielczarek, D., Sikorski, P., Archiciński, P., Ciężkowski, W., Zaniewska, E., Chormański, J., 2023. The Use of an Airborne Laser Scanner for Rapid Identification of Invasive Tree Species Acer negundo in Riparian Forests. Remote Sens. 15. https://doi.org/10.3390/rs15010212.

Murray, B.A., Coops, N.C., Winiwarter, L., White, J.C., Dick, A., Barbeito, I., Ragab, A., 2024. Estimating tree species composition from airborne laser scanning data using point-based deep learning models. ISPRS J. Photogramm. Remote Sens. 207, 282–297. https://doi.org/10.1016/j.isprsjprs.2023.12.008.

Nauber, T., Hodač, L., Wäldchen, J., Mäder, P., 2024. Parametrization of biological assumptions to simulate growth of tree branching architectures. Tree Physiol. 44. https://doi.org/10.1093/treephys/tpae045.

Nilsson, M., Nordkvist, K., Jonzén, J., Lindgren, N., Axensten, P., Wallerman, J., Egberth, M., Larsson, S., Nilsson, L., Eriksson, J., Olsson, H., 2017. A nationwide forest attribute map of Sweden predicted using airborne laser scanning data and field data from the National Forest Inventory. Remote Sens. Environ. 194, 447–454. https://doi.org/10.1016/j.rse.2016.10.022.

Noordermeer, L., Ørka, H.O., Gobakken, T., 2023. Imputing stem frequency distributions using harvester and airborne laser scanner data: a comparison of inventory approaches. Silva Fenn. 57, 1–20.

Onishi, M., Ise, T., 2021. Explainable identification and mapping of trees using UAV RGB image and deep learning. Sci. Rep. 11, 1–15. https://doi.org/10.1038/s41598-020-79653-9.

Oubara, A., Wu, F., Amamra, A., Yang, G., 2022. Survey on Remote Sensing Data Augmentation: Advances, Challenges, and Future Perspectives, in: Senouci, M.R., Boulahia, S.Y., Benatia, M.A. (Eds) Advances in Computing Systems and Applications. CSA 2022. Lecture Notes in Networks and Systems, Vol 513. Springer, Cham., pp. 95–104. DOI: 10.1007/978-3-031-12097-8_9.

Persson, H.J., Olofsson, K., Holmgren, J., 2022. Two-phase forest inventory using very-high-resolution laser scanning. Remote Sens. Environ. 271, 112909. https://doi.org/10.1016/j.rse.2022.112909.

Pires, R. de P., Lindberg, E., Persson, H.J., Olofsson, K., Holmgren, J., 2024. Mobile laser scanning as reference for estimation of stem attributes from airborne laser scanning. Remote Sens. Environ. 315, 114414. DOI: 10.1016/j.rse.2024.114414.

Pires, R. de P., Olofsson, K., Persson, H.J., Lindberg, E., Holmgren, J., 2022. Individual tree detection and estimation of stem attributes with mobile laser scanning along boreal forest roads. ISPRS J. Photogramm. Remote Sens. 187, 211–224. DOI: 10.1016/j.isprsjprs.2022.03.004.

Puliti, S., Breidenbach, J., Astrup, R., 2020. Estimation of forest growing stock volume with UAV laser scanning data: Can it be done without field data? Remote Sens. 12, 1245. https://doi.org/10.3390/RS12081245.

Puliti, S., Mclean, J.P., Cattaneo, N., Fischer, C., Astrup, R., 2023a. Tree height-growth trajectory estimation using uni-temporal UAV laser scanning data and deep learning. For. an Int. J. for. Res. 96, 37–48. https://doi.org/10.1093/forestry/cpac026.

Puliti, S., Pearse, G., Surový, P., Wallace, L., Hollaus, M., Wielgosz, M., Astrup, R., 2023b. FOR-instance: a UAV laser scanning benchmark dataset for semantic and instance segmentation of individual trees. arXiv Prepr. arXiv2309.01279.

Qian, C., Yao, C., Ma, H., Xu, J., Wang, J., 2023. Tree Species Classification Using Airborne LiDAR Data Based on Individual Tree Segmentation and Shape Fitting. Remote Sens. 15. https://doi.org/10.3390/rs15020406.

Schiefer, F., Kattenborn, T., Frick, A., Frey, J., Schall, P., Koch, B., Schmidtlein, S., 2020. Mapping forest tree species in high resolution UAV-based RGB-imagery by means of convolutional neural networks. ISPRS J. Photogramm. Remote Sens. 170, 205–215. https://doi.org/10.1016/j.isprsjprs.2020.10.015.

Seidel, D., Annighöfer, P., Thielman, A., Seifert, Q.E., Thauer, J.H., Glatthorn, J., Ehbrecht, M., Kneib, T., Ammer, C., 2021. Predicting Tree Species From 3D Laser Scanning Point Clouds Using Deep Learning. Front. Plant Sci. 12, 1–12. https://doi.org/10.3389/fpls.2021.635440.

Shi, Y., Skidmore, A.K., Wang, T., Holzwarth, S., Heiden, U., Pinnel, N., Zhu, X., Heurich, M., 2018a. Tree species classification using plant functional traits from LiDAR and hyperspectral data. Int. J. Appl. Earth Obs. Geoinf. 73, 207–219. https://doi.org/10.1016/j.jag.2018.06.018.

Shi, Y., Wang, T., Skidmore, A.K., Heurich, M., 2018b. Important LiDAR metrics for discriminating forest tree species in Central Europe. ISPRS J. Photogramm. Remote Sens. 137, 163–174. https://doi.org/10.1016/j.isprsjprs.2018.02.002.

Söderberg, J., Wallerman, J., Almäng, A., Möller, J.J., Willén, E., 2021. Operational prediction of forest attributes using standardised harvester data and airborne laser scanning data in Sweden. Scand. J. for. Res. 36, 306–314. https://doi.org/10.1080/02827581.2021.1919751.

Sothe, C., De Almeida, C.M., Schimalski, M.B., La Rosa, L.E.C., Castro, J.D.B., Feitosa, R. Q., Dalponte, M., Lima, C.L., Liesenberg, V., Miyoshi, G.T., Tommaselli, A.M.G., 2020. Comparative performance of convolutional neural network, weighted and conventional support vector machine and random forest for classifying tree species using hyperspectral and photogrammetric data. Giscience Remote Sens. 57, 369–394. https://doi.org/10.1080/15481603.2020.1712102.

Straker, A., Puliti, S., Breidenbach, J., Kleinn, C., Pearse, G., Astrup, R., Magdon, P., 2023. Instance segmentation of individual tree crowns with YOLOv5: A comparison of approaches using the ForInstance benchmark LiDAR dataset. ISPRS Open J. Photogramm. Remote Sens. 9, 100045. https://doi.org/10.1016/j.ophoto.2023.100045.

Takhtkeshha, N., Mandlburger, G., Remondino, F., Hyyppä, J., 2024. Multispectral Light Detection and Ranging Technology and Applications: A Review. Sensors 24. https://doi.org/10.3390/s24051669.

Terryn, L., Calders, K., Disney, M., Origo, N., Malhi, Y., Newnham, G., Raumonen, P., Å kerblom, M., Verbeeck, H., 2020. Tree species classification using structural features derived from terrestrial laser scanning. ISPRS J. Photogramm. Remote Sens. 168, 170–181. DOI: 10.1016/j.isprsjprs.2020.08.009.

Wang, J., Jiang, Y., 2024. A Hybrid convolution neural network for the classification of tree species using hyperspectral imagery. PLoS One 19, e0304469. https://doi.org/10.1371/journal.pone.0304469.

Wu, J., Chen, L., Wang, J., Li, Y., Chen, E., Zhang, X., 2024. A novel framework combining band selection algorithm and improved 3D prototypical network for tree species classification using airborne hyperspectral images. Comput. Electron. Agric. 219, 108813. https://doi.org/10.1016/j.compag.2024.108813.

Xi, Z., Hopkinson, C., Rood, S.B., Peddle, D.R., 2020. See the forest and the trees: Effective machine and deep learning algorithms for wood filtering and tree species classification from terrestrial laser scanning. ISPRS J. Photogramm. Remote Sens. 168, 1–16. https://doi.org/10.1016/j.isprsjprs.2020.08.001.

Xiang, B., Wielgosz, M., Kontogianni, T., Peters, T., Puliti, S., Astrup, R., Schindler, K., 2023. Automated forest inventory: analysis of high-density airborne LiDAR point clouds with 3D deep learning. DOI: 10.1016/j.rse.2024.114078.

Xu, Q., Hou, Z., Maltamo, M., Tokola, T., 2014a. Retrieving suppressed trees from model-based height distribution by combining high-and low-density airborne laser scanning data. Can. J. Remote Sens. 40, 233–242. https://doi.org/10.1080/07038992.2014.935933.

Xu, Q., Hou, Z., Maltamo, M., Tokola, T., 2014b. Calibration of area based diameter distribution with individual tree based diameter estimates using airborne laser scanning. ISPRS J. Photogramm. Remote Sens. 93, 65–75. https://doi.org/10.1016/j.isprsjprs.2014.03.005.

Xu, S., Wang, R., Shi, W., Wang, X., 2024. Classification of Tree Species in Transmission Line Corridors Based on YOLO v7. Forests 15, 1–17. https://doi.org/10.3390/f15010061.

Yu, X., Hyyppä, J., Litkey, P., Kaartinen, H., Vastaranta, M., Holopainen, M., 2017. Single-sensor solution to tree species classification using multispectral airborne laser scanning. Remote Sens. 9, 1–16. https://doi.org/10.3390/rs9020108.

Zhang, H., Wang, C., Tian, S., Lu, B., Zhang, L., Ning, X., Bai, X., 2023. Deep learning-based 3D point cloud classification: A systematic survey and outlook. Displays 79, 102456. https://doi.org/10.1016/j.displa.2023.102456.